JOURNAL OF MATERIALS SCIENCE 11 (1976) 656–664

Effect of back-stress on cyclic stress-strain behaviour of a quenched and tempered low alloy steel

K. TANAKA, S. MATSUOKA
Fatigue Testing Division, National Research Institute for Metals, 2-3-12 Nakameguro, Meguroku, Tokyo 153, Japan

Low cycle fatigue was considered in relation to back-stress hardening. Cyclic stress–strain behaviours under controlling strain and stress conditions were investigated for a quenched and tempered low alloy steel which contained cementite particles. The cyclic stress–strain states obtained by the two prescribed tests were uniquely described using a parameter which reflected the cumulative reversible plastic work associated with the back-stress hardening. It was suggested that the effect of back-stress hardening on cyclic deformation should appear directly on the cyclic stress–strain curves defined as the loci of the tips of stable hysteresis loops. The initial slopes of the cyclic stress–strain curves for several steels were demonstrated to coincide with the theoretical work-hardening rates calculated on the basis of back-stress hardening due to the included carbide particles. Finally, the Manson–Coffin law was explained from the view that the surface damage would progress in parallel with the structure change in the bulk according to the persistency of slips resulting from the reversible back-stress hardening.

1. Introduction

The plastic work dissipated during fatigue failure of metals is usually much larger than that required for failure in the monotonic tension test [1]. This probably follows from the fact that most of the plastic flow in cyclic deformation occurs in a reversible way, and that only a small fraction of the deformation results from the irreversible slip which ultimately leads to fatigue failure. Thus, the reversibility of the phenomenon is more remarkable as a controlling factor for dislocation arrangements and movements in the bulk material under cyclic loading than the small irreversibility.

It is natural to consider that the reversibility of the slips is intimately related to the reversibility or "recoverability' of the energy storage mechanisms associated with cyclic deformation. The mechanisms have been discussed in terms of the Bauschinger effect [2]. Orowan proposed two generalized types of the effect, namely back-stress effect and "obstacle hardening" effect [3]. Orowan emphasized that back-stress hardening, developed in a forward direction, ought to be wiped out to a large extent by reversed plastic deformation, and that it would therefore give rise to a "permanent" softening effect. Wilson termed this hardening "reversible work-hardening" because of its reversibility [4]. The obstacle hardening is caused by the random distribution of obstacles [3]. A dislocation, which is stopped by a row of obstacles under a forward applied stress, can move by a lower reverse stress, because the row of obstacles in the rear of the dislocation is unlikely to consist of obstacles as strong and as closely packed as the one immediately in front of the dislocation.

Kettunen and Kocks [5] studied in detail the effect of the obstacle hardening mechanism on cyclic hardening behaviour in copper single crystals under prescribed stress and strain amplitudes*. Assuming the existence of a critical Orowan stress at which any dislocation can penetrate indefinitely throughout the array of obstacles, they concluded that cyclic deformation can be divided into two regions; one below the critical yield strength where

*Kettunen and Kocks termed the contribution of the obstacle hardening during cyclic deformation as "cyclic hardening" [5].

straining is controlled by obstacle hardening; the other above the yield strength where straining is controlled by "instantaneous" work-hardening occurring during the half-cycle in question. Kettunen and Kocks found that the critical yield strength corresponded to a shear strain amplitude of about 2×10^{-3}.

Although Kettunen and Kocks investigated the problem of the obstacle hardening, they also conducted tests on ordinary low-cycle fatigue under a strain amplitude of 2×10^{-3} to 10^{-1}, in which the "instantaneous" work-hardening prevails. In this region, the back-stress hardening mechanism will be mainly operative as a cause of the reversibility of deformation during cycling tests, the mechanism being significant particularly when the obstacles are strong [4]. The present work was undertaken to examine the important role of the back-stress on the cyclic stress–strain behaviour of material. The experiments were carried out mainly on a quenched and tempered low alloy steel which contained dispersed cementite particles.

2. Effect of back-stress on the stress–strain curve

In the case of a dispersion-hardened material, the sources of back-stress are geometrically definite, and the amount of back-stress is known to increase linearly as plastic straining develops [6, 7]. Fig. 1 shows a schematic feature of a hysteresis loop for a dispersion-hardened material at the initial cycle of deformation of the strain cycling test. For simplicity, the work-hardening caused by other mechanisms than the back-stress mechanism is omitted and the frictional stress, σ_0, is assumed to be constant*. At the first forward deformation the material yields at 0 and work-hardens linearly as illustrated by 0B in Fig. 1. On unloading from A to C and reloading in the reverse direction, yielding will start at stress D, where $0_1A = 0_1D$, since the back stress, 0_1A, assists the reverse deformation by the same amount. After yielding, linear hardening occurs until the strain increases to twice the prescribed strain amplitude, $2\epsilon_{pa}$. Since the work-hardening rates in both deformations should be the same, the influence from the back-stress developed by the forward direction can be recovered at the same strain in the reverse direction. After the attainment of the applied stress to the frictional stress at point 0_2, the accumulation of back-stress in the reverse direction occurs along 0_2E in the same manner as that in the forward deformation. On unloading from E to F and reloading from F in the forward direction, the recovery of back-stress occurs up to point 0_4 where the stress state returns to the starting point 0.

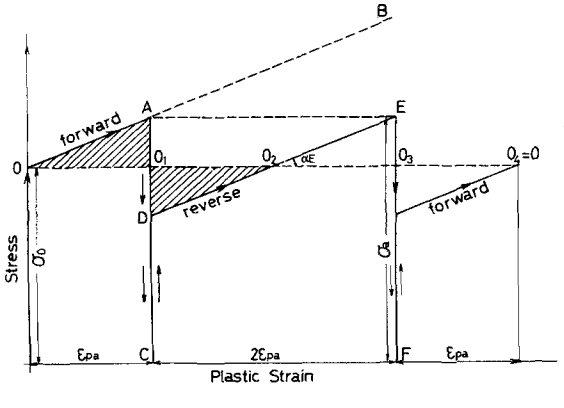

Figure 1 Schematic representation of a hysteresis loop at the first cycling of a back-stress hardened material.

These processes should repeat in a reversible way throughout cyclic deformations, if the frictional stress term was held constant. However, actual materials show cyclic hardening or cyclic softening behaviour because of changes in the dislocation microstructure. In the case of dispersion-hardened material, the structure change in the matrix can be attributed to two causes. One is due to the plastic work dissipated to overcome frictional forces†. This is essentially irreversible and the resulting structure change should effect the work-hardening additive in proportion to the cumulative plastic work, in the same manner as that in the monotonic loading. The other is related to the stored energy associated with the back-stress hardening, which is proportional to the product of ϵ_{pa}^2 and Young's modulus of the material, E, since it is expressed by the area $0A0_1 = 0_1D0_2$. The alternate accumulation-and-recovery process of back-stress during cyclic load-

*Here the obstacle hardening is discarded and σ_0 corresponds to the critical Orowan stress in the Kuttunen and Kock's conception.

†The term dissipation energy is used here to refer to the work required to plastically deform the matrix alone. Part of this work might be stored in the matrix. However, when it is not recovered by plastic deformation in the reverse direction, it can be treated as dissipative work for all practical purposes.

ing would activate the to-and-fro movement of glide dislocations in the matrix, which would result in the characteristic fatigue structure (back-stress effect). This process would operate essentially to force the structure into a state similar to that when the deformation temperature was enhanced. This idea follows from the analogy of the to-and-fro movement of dislocations with the thermal fluctuation of dislocations. The latter occurs in the order of an atomic distance, while the former does so on a larger scale. Hence, the reaction of the two mechanisms, the monotonic work-hardening and the back-stress effect, will act on the structure change of cyclically-deformed materail principally in a competitive way. Namely, the former will tend to increase the frictional stress, while the latter will tend to decrease it.

The literature shows that quenched and tempered steels with medium carbon content cyclically soften drastically [8, 9]. These materials have a tempered martensitic structure with dispersed carbide particles. It is proposed, from the view advanced above, that the cyclic softening behaviour in such materials would result from a decrease in the frictional stress throughout cyclic deformation according to the dominant operation of the back-stress effect associated with the carbide particles.

Consequently, the following would be expected:

(1) The transient behaviour of the stress–strain relations during cyclic deformation from the monotonic stress–strain curve to the steady-state cyclic stress–strain curve, could be adequately expressed using a parameter related to the reversible plastic work resulting from the back-stress. rather than that related to the total dissipated plastic work.

(2) The work-hardening of these materials should be linear and the hardening rate should agree with that calculated on the basis of the hardening theory developed by Tanaka and Mori [6, 10]. This would be clearly envisaged on the stress–strain curve at the stable state of cyclic deformation where the work-hardening due to the other causes than back-stress hardening would be excluded, since the monotonic work-hardening would be in saturation.

(3) The back-stress field is essentially uniform in the entire specimen, but the field at the surface of the specimen varies in the order of interparticle spacing [7]. The variation of back-stress would induce inhomogeneous slips at the surface, which would become the embryo of fatigue cracks. However, the growth of the embryonic slips into the fatigue cracks would be promoted by the persistency or reversibility of deformation due to the back-stress effect. The Manson–Coffin law should be explained on this basis.

The experiment was based on these hypotheses.

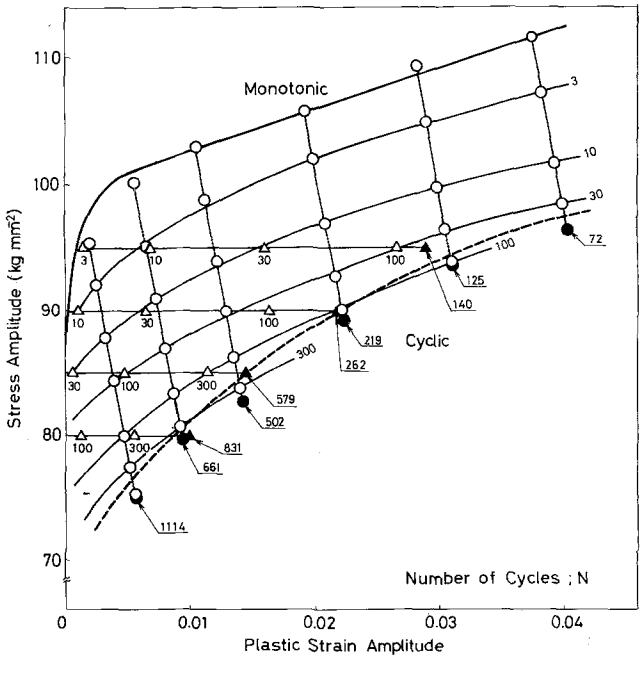

Figure 2 Monotonic and cyclic stress–strain curves for 600° C tempered JIS SNCM8 steel. Full curve; monotonic, dotted curve; cyclic at half the fatigue life. Traces of tips after the indicated number of cycling by (○) strain controlling tests, (△) by stress controlling tests. Filled marks correspond to the states at fatigue failure.

3. Cyclic softening behaviour of quenched and tempered JIS SNCM8 steel

The starting material was 35 mm diameter hot-rolled bars of JIS SNCM8 steel, which corresponds to 4340 steel in SAE grade. The ladle analysis of the steel showed 0.40% C, 1.68% Ni, 0.68% Cr, 0.18% Mo, with minor trace elements. After rough machining, most specimens were quenched from 845° C and tempered at temperatures between 200 and 600° C in order to develop various strength levels. The heat-treatments provided tempered martensitic structures with various ranges of sizes of dispersed particles. A small number of specimens were annealed at 660° C to obtain a pearlitic structure. The 600° C tempered specimens were mainly employed for the tests. The specimens were cylindrical with a reduced central portion, 10 mm in diameter, containing a 1 mm parallel gauge length.

Tests were conducted under two prescribed loading conditions using an MTS electrohydraulic system. The strain cycling test was carried out at a completely reversed total strain range, and the stress cycling test was performed at a constant load range. In the case of stress cycling, the specimen suffered cyclic creep, even when the mean stress was nominally zero. The effect occurred immediately after the test was begun and accelerated as the test proceeded until eventually the specimen was necked in the gauge length. This was attributed to the fact that, although the load limits were equal and opposite, the true stress limits in tension and compression were not the same [11]. Thus, cyclic creep in reversed loading was prevented by slight adjustment of the load limits, as the mean strain, monitored by an extensometer, was held constant at almost zero throughout the test.

The test results for the 600° C tempered steel are shown in Fig. 2 as a plot of loci of tips of stress–strain hysteresis loops from specimens subjected to different levels of cyclic stress or strain. The upper-most curve is the monotonic stress–strain curve. The six vertical lines (○) are for strain cycling tests and the four horizontal ones (△) are for stress cycling tests. The numbers in the figure are the number fo cycles. At the strain cycling tests, the strength decreased drastically at the initial few cycles and the hysteresis loops rapidly settled down to an almost stable state. As is well known [1], most of the fatigue life is spent at the stable state, during which fatigue crack propagation occurs and results in the fracture of the specimen at a point indicated by a solid mark (●, ▲). The dotted curve is the cyclic stress–strain curve, which is constructed in a conventional manner by the trace of tips of the loops at approximately half the fatigue life chosen as representative for the stable behaviour. Contrary to this, at the stress cycling tests, the work-softening behaviour was gradual and the stable state was not so

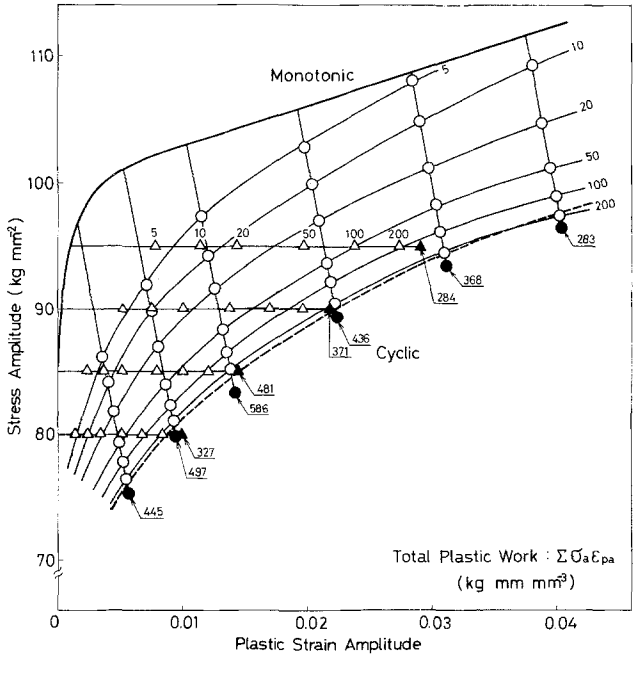

Figure 3 Replotting of Fig. 2 as a function of cumulative plastic work.

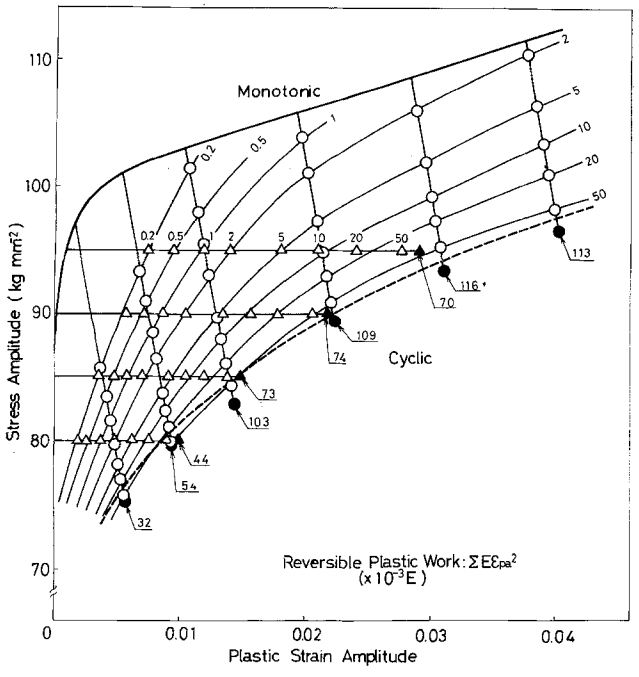

Figure 4 Replotting of Fig. 2 as a function of cumulative reversible plastic work.

steady as that in the case of the strain cycling test.

It is evident from Fig. 2 that the cyclic stress–strain states at a given number of cycles were not the same between the results of two prescribed loading conditions. The points of the stress cycling test in the figure are situated outside the corresponding traces of the results on equal reversal testings under strain cycling and, at an equal reversal, the stress cycling test gave a state of higher stress amplitude and smaller plastic strain amplitude than the strain cycling test. The discrepancy comes, of course, from the fact that the magnitudes and histories of plastic work given to specimens were different for the two loading conditions, even when the number of cycles was equal.

The cyclic stress-strain states in Fig. 2 are replotted in Figs. 3 and 4 as a function of two kinds of cumulative plastic work. Fig. 3 is for the dissipated plastic work, which is represented by the cumulative plastic work, $\Sigma\sigma_a\epsilon_{pa}$, where σ_a is the stress amplitude and the summation is performed from the first number of cycling to the prescribed one. The dissipated plastic work per half cycle is expressed by the area $0_1 0_3 FC$ in Fig. 1, which can be approximately replaced by the area AEFC. Fig. 4 is for the reversible plastic work, which is represented by the cumulative plastic work, $\Sigma E\epsilon_{pa}^2$. This energy per half cycle is shown by the area $0A0_1 = 0_1 0_2 D$ in Fig. 1 and proportional to $E\epsilon_{pa}^2$.

These figures show that the cumulative plastic works are good variables which are uniquely indicative of the cyclic stress–strain states obtained by the two prescribed loading conditions. The goodness of fit of the data for two loading conditions appears to be far better in Fig. 4 than in Fig. 3. This suggests that the reversible plastic work is more appropriate as a state variable in determining the cyclic stress–strain relations than is the total plastic work.

4. Work-hardening behaviour in cyclic stable states

Fig. 5a shows the tensile half of stable hysteresis loops for five 600° C tempered specimens tested under cyclic straining. The points are the tips of the loops and the cyclic stress–strain curve is obtained by connecting the points. On the basis of the back-stress hardening effect illustrated in Fig. 1, the hardening behaviour in Fig. 5a can be explained as schematically represented in Fig. 5b.

It is likely that the saturated microstructure developed during the steady state is stable and that it does not depend strongly on the cycling history. Thus, it is assumed that the specimens subjected to different strain amplitudes have the same constant frictional stress, σ_0, at the stable states as shown by the dotted line $00'$ in Fig. 5b. Although there is no direct justification for this assumption, without

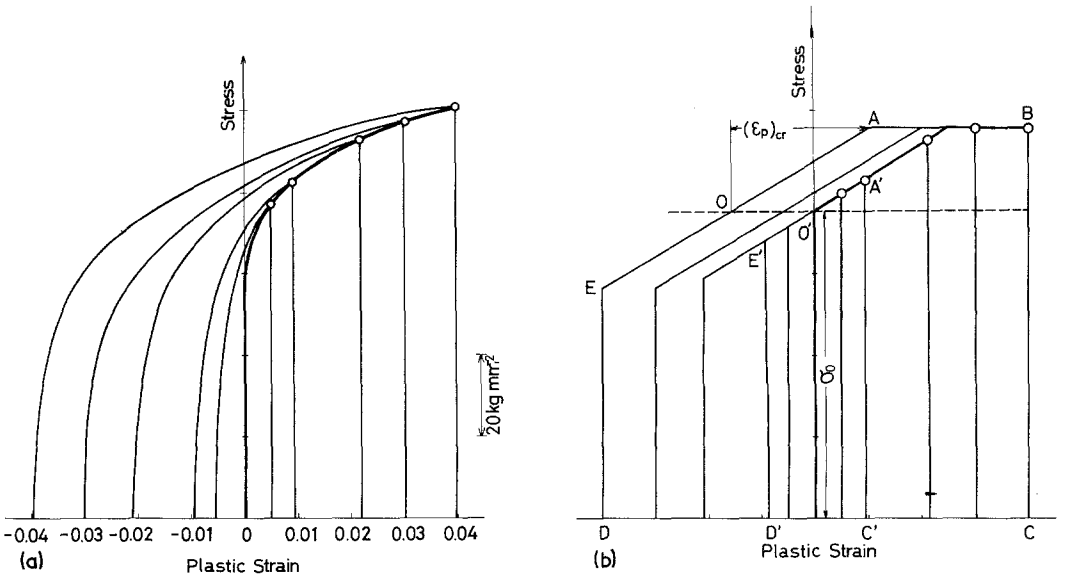

Figure 5 (a) Tensile half of stable hysteresis loops for 600° C tempered JIS SNCM8 steel. The traces of the points form the cyclic stress–strain curve. (b) Schematic illustration of (a).

it, it may be impossible to explain self-consistently the complete reversion of the same patterns of hysteresis loops during the stable cyclic deformation.

When the applied strain amplitude was small, the hysteresis loop had the shape, D′E′0′A′C′, where the back-stress due to the dislocation-trapping carbide particles would have affected the cyclic behaviour in the same way as that exhibited in Fig. 1. The recovery process of the back stress developed in the compressive deformation in the region E′0′, and accumulated in the tensile deformation in region 0′A′. When the strain amplitude was large, the hysteresis loop had the shape, DE0ABC. In this case the accumulation of back-stress would have become saturated at some critical plastic strain, $(\epsilon_p)_{cr}$, because the amount of internal stress around the particles became so large that such stress-relieving mechanisms as cross-slipping of dislocations and/or plastic deformation of particles would operate [6]. Thus the breakdown of hardening would have occurred in the region AB after the linear hardening, expressed by the region E0A of the same slope as that of line E′A′. Therefore the tips of the loops resulting from the deformation of strain amplitude below the critical strain, would be along the linear hardening line starting from the point 0′, and those above the critical strain would be on the flat line AB.

The actual situations were more complicated. The early state of deformation, corresponding to the portion DE0 or D′E′0′ in Fig. 5b, appeared parabolic, and the plastic deformation initiated at a stress less than point E or E′ as represented in Fig. 5a. The phenomenon was probably caused by the obstacle-hardening mechanism proposed by Orowan [3]. The breakdown of back-stress did not take place so drastically as modelled in Fig. 5b. However, in principle, it can be concluded from the schematic representation of the cyclic stable behaviour that the back-stress hardening affecting the construction of the fatigue substructure should be envisaged clearly in the cyclic stress–strain curve rather than in the monotonic stress–strain curve. Evidence in favour of this view will be seen in the following.

Fig. 6 shows the respective cyclic and monotonic stress–strain curves for JIS SNCM8 steel heat-treated in five different ways. The upper four curves are for quenched and tempered materials with different tempering temperatures, respectively, and the lowest one is for annealed material at 660° C. The hardening behaviours in the monotonic stress–strain curves are dependent on these materials. Contrary to this, those in the cyclic stress–strain curves have a similarity. As was expected, the experimental hardening rates in the latter curves, except for 200° C tempered steel, compare well with the theoretical ones as represented by the dot-dashed curves in the same figure. On

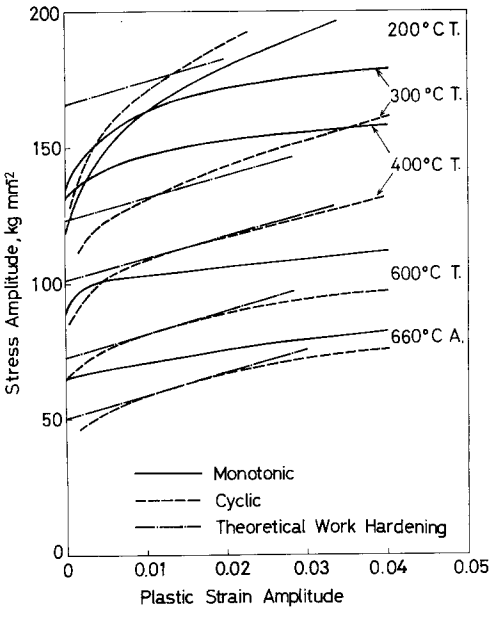

Figure 6 Monotonic and cyclic stress–strain curves for JIS SNCM8 steel with five different heat-treatments (T, quenched and tempered; A, annealed).

the basis of a linear hardening model, the theoretical hardening rates, $d\sigma_a/d\epsilon_{pa}$, were obtained as [10]

$$d\sigma_a/d\epsilon_{pa} = \alpha E$$

with

$$\alpha = \frac{7-5\nu}{10(1-\nu^2)} \frac{f}{(1-f)} . \quad (1)$$

Here ν is the Poissons ratio of iron equal to 0.3 and f is the volume fraction of carbides and taken as 0.062, which is calculated according to the assumption that the matrix contains the equilibrium carbon content of ferrite in a 0.40% carbon alloy.

In Fig. 6, the 200° C tempered steel showed an anomalous tendency in the cyclic behaviour compared with other steels, and the experimental curve provided a hardening rate about three times higher than the theoretical one*. This is probably related to the character of the precipitated carbides. In the case of 200° C tempering, the carbides are composed of cementite and epsilon carbides, while after tempering at 300° C or above, they are almost completely of cementite [12]. Thus it is likely that the dissolution of epsilon carbides during cyclic deformation caused the anomaly, and the sources of back-stress, other than the precipitated carbides, would be originated.

5. Fatigue damage

The cyclic–strain behaviour should reflect the structure changes in a bulk specimen. However, fatigue failure is known to start from the surface. Examples of this are shown in Fig. 7. This figure shows the optical photographs for the replicas of the surface on three specimens of 600° C tempered SNCM8 steel tested under three different conditions. The growth stages of the surface damage appeared quite similar among three specimens when the parameters of $\Sigma E\epsilon_{pa}^2$ were coincident, even though the numbers of cycles or the values of $\Sigma\sigma_a\epsilon_{pa}$ were different.

This fact suggests that the surface damage as well as the bulk damage is controlled by the back-stress effect. Thus it will be reasonable to assume that failure occurs when some critical constant amount of cumulative reversible plastic work is reached. Then the criterion would be described by

$$\Sigma\alpha E\epsilon_{pa}^2 = \text{constant} \quad (2)$$

since the reversible plastic work per cycle due to the back-stress effect is expressed by the area $0A0_1$ ($= \alpha E\epsilon_{pa}^2/2$) in Fig. 1. In the case of the strain controlled test, since most of the test took place at the stable state, the plastic strain amplitude and the hardening parameter, α, could be taken as constant. Hence Equation 2 would be rewritten by

*In Fig. 6, the 200° C tempered steel appears to cyclically harden, i.e. the cyclic stress–strain curve is higher than the monotonic one. However, this is only apparent, because the plastic strain amplitudes were found to increase with progress of cycling. The discrepancy in the behaviour of the steel in Fig. 6 comes from the fact that the monotonic stress–strain curve of the steel in the figure represents only the tensile half, in spite of the fact that the strength of the steel in compression was higher than that in tension.

Figure 7 Replicas of fatigued surface in 600° C tempered JIS SNCM8 steels tested by three different loading conditions. The loading axis is vertical, ×400. Strain controlled at a total strain amplitude of 0.04: (a) before testing; (b) after 12 cycles, $\Sigma\sigma_a\epsilon_{pa} = 18$ (kg mm mm^{-3}), $\Sigma E\epsilon_{pa}^2 = 5$ ($\times 10^{-3}E$); (c) after 43 cycles, $\Sigma\sigma_a\epsilon_{pa} = 70$, $\Sigma E\epsilon_{pa}^2 = 20$; (d) after 103 cycles, $\Sigma\sigma_a\epsilon_{pa} = 180$, $\Sigma E\epsilon_{pa}^2 = 50$. Strain controlled at a total strain amplitude of 0.025: (e) before testing; (f) after 80 cycles, $\Sigma\sigma_a\epsilon_{pa} = 50$, $\Sigma E\epsilon_{pa}^2 = 4.3$; (g) after 270 cycles, $\Sigma\sigma_a\epsilon_{pa} = 200$, $\Sigma E\epsilon_{pa}^2 = 18$; (h) after 716 cycles, $\Sigma\sigma_a\epsilon_{pa} = 500$, $\Sigma E\epsilon_{pa}^2 = 50$. Stress controlled at a stress amplitude of 90 kg mm^{-2}: (i) before testing; (j) after 51 cycles, $\Sigma\sigma_a\epsilon_{pa} = 5.3$; (k) after 95 cycles; $\Sigma\sigma_a\epsilon_{pa} = 130$, $\Sigma E\epsilon_{pa}^2 = 20$; (l) after 160 cycles, $\Sigma\sigma_a\epsilon_{pa} = 250$, $\Sigma E\epsilon_{pa}^2 = 53$. Note that the growth stages of surface damage are similar among three specimens when they have similar values of $\Sigma E\epsilon_{pa}^2$.

a
b
c
d
e
f
g
h
i
j
k
l

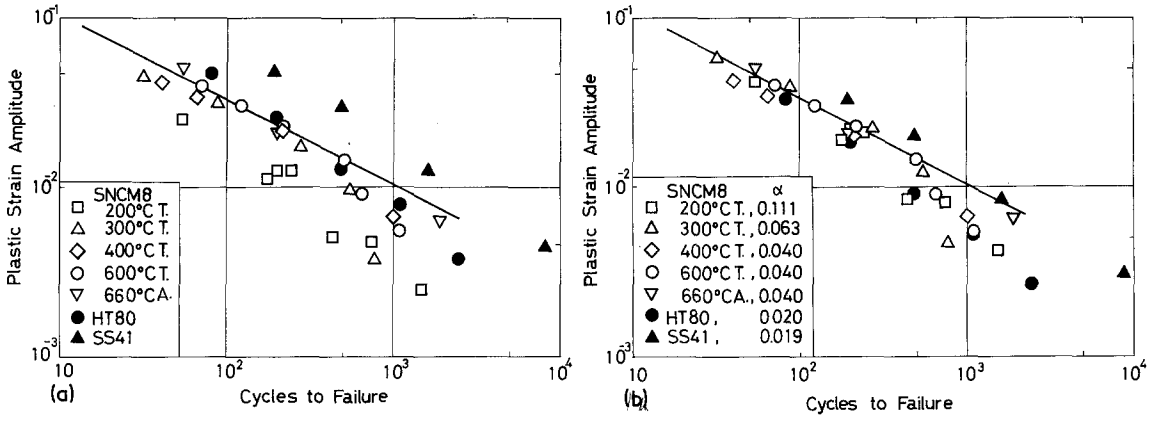

Figure 8 (a) Manson–Coffin plots for five JIS SNCM8 steels in the present work and for two other steels. [14] (b) The corrected plots by the hardening parameter, α. The data are normalized to those for 600° C tempered SNCM8 steel.

using the cyclic life, N_f, as

$$N_f \alpha E \epsilon_{pa}^2 = \text{constant, or } N_f^{1/2} \alpha^{1/2} E_1^{1/2} \epsilon_{pa} = \text{constant,} \quad (3)$$

which is the form of the Manson–Coffin law. This equation is also derived by Martin [13] according to a physical ground somewhat different from that in the present paper.

Fig. 8a shows the Manson–Coffin plot of results on the cyclic strain tests for SNCM8 steels examined in the present work and for two other steels [14]; HT80 (high tension steel, 0.12C–1.05Ni–0.45Cr–0.31Mo, quenched and tempered at 550° C) and SS41 steel (mild steel, 0.17C, annealed). The data in Fig. 8a are replotted in Fig. 8b by normalizing the strain amplitude as $(\alpha/\alpha_0)^{1/2} \epsilon_{pa}$, where α is the hardening factor measured in the experimental cyclic stress–strain curves, and α_0 is that for 600° C tempered SNCM8 steel. These values of α are shown in Fig. 8b. The agreement between the points for 600° C tempered steel with those for other steels is very good. This fact suggests that Equation 3 is generally in the right direction.

Acknowledgements

The authors are indebted to Professor T. Mori in Tokyo Institute of Technology and, to Professor S. Yoshida in National Research Institute for Metals, for helpful discussions and suggestions. Thanks are due to the able assistance of K. Miyazawa and F. Kouzo in testing and drafting.

References

1. JODEAN MORROW, ASTM Spec. Tech. Pub. No. 378 (1964) 45.
2. A. ABEL and H. MUIR, *Phil. Mag.* **26** (1972) 489.
3. E. OROWAN, "Internal Stresses and Fatigue in Metal" (Elsevier, New York, 1959) p. 59.
4. D. V. WILSON, *Acta Met.* **13** (1965) 807.
5. P. O. KETTUNEN and U. F. KOCKS, *ibid* **20** (1972) 95.
6. K. TANAKA and T. MORI, *ibid* **18** (1970) 931.
7. T. MORI and K. TANAKA, *ibid* **21** (1973) 571.
8. R. W. SMITH, M. H. HIRSHBERG and S. S. MANSON NASA Tech. Note D-1574, April (1963).
9. R. W. LANDGRAF, JODEAN MORROW and T. ENDO, *J. Materials* **4** (1969) 176.
10. K. TANAKA and S. MATSUOKA, *Acta Met.* **22** (1974) 22.
11. P. P. BENHAM, *J. Inst. Metals* **89** (1961–62) 328.
12. G. V. KURDJUMOV, *J. Iron Steel Inst.* **195** (1960) 26.
13. D. E. MARTIN, *J. Basis Eng., Trans. ASME (D)* **83** (1961) 565.
14. S. MATSUOKA, K. TANAKA and M. KAWAHARA, unpublished work.

Received 18 August and accepted 3 October 1975.